OPEN

NPG Asia Materials (2016) 8, e317; doi:10.1038/am.2016.138
www.nature.com/am

ORIGINAL ARTICLE

# The dual actions of modified polybenzimidazole in taming the polysulfide shuttle for long-life lithium–sulfur batteries

Gaoran Li[1], Can Wang[1], Wenlong Cai[2], Zhan Lin[1], Zhoupeng Li[1] and Shanqing Zhang[3]

**The development of lithium–sulfur (Li–S) batteries is of practical significance to meet the rapidly escalating demand for advanced energy storage technologies with long life and high-energy density. However, the dissolution and shuttling of the intermediate polysulfides (PS) initiates the loss of active sulfur and the poisoning of the lithium anode, leading to unsatisfactory cyclability and consequently hinders the commercialization of Li–S batteries. Herein, we develop a facile strategy to tame the PS dissolution and the shuttling effect in the Li–S system by introducing a modified polybenzimidazole (mPBI) with multiple functions. As a binder, the excellent mechanical property of mPBI endows the sulfur electrode with strong integrity and, therefore, results in high sulfur loading (7.2 mg cm$^{-2}$), whereas the abundant chemical interaction between mPBI and PS affords efficient PS adsorption to inhibit sulfur loss and prolong battery life. As a functional agent for the separator, the mPBI builds a PS shield onto the separator to block PS's migration to further suppress the PS shuttling. The dual actions of mPBI confer an excellent performance of 750 mAh g$^{-1}$ (or 5.2 mAh cm$^{-2}$) after 500 cycles at C/5 on the Li–S battery with an ultralow capacity fading rate of 0.08% per cycle.**

*NPG Asia Materials* (2016) **8,** e317; doi:10.1038/am.2016.138; published online 7 October 2016

## INTRODUCTION

Li-ion batteries, which are typically composed of a transitional metal oxide cathode and a graphite anode,[1–3] are unable to fulfill the increasing demand for advanced energy storage technologies with long life and high-energy density owing to the rapid development of various portable electronics and electric vehicles.[4,5] Lithium–sulfur (Li–S) batteries are considered to be the most promising candidate to meet such needs owing to their inherent merits such as their high theoretical energy density (five times higher than Li-ion batteries, that is, up to 2500 Wh kg$^{-1}$), low cost and environmental friendliness.[6] However, Li–S batteries are plagued with drawbacks, including poor cyclability, low coulombic efficiency and insufficient utilization of active material, which can be ascribed to the poor electric and ionic conductivity of the active sulfur material, dissolution of polysulfide (PS) intermediates in ether-based electrolyte and significant volumetric change (that is, ≈76%) during charge–discharge processes.[7] Despite the great application potential of Li–S batteries in portable electronics, electric vehicles and grid electrical energy storage, these obstacles must be overcome before their commercialization.

Numerous approaches have attempted to address these problems. A significant effort was focused on designing various conductive network/sulfur composites, including nano-structured carbon materials, metal oxides and conductive polymers, among others, to improve electric conductivity and sulfur retention.[8,9] Yet, in addition to the unsuitable complexity and high cost of these strategies for large-scale manufacturing, they do not address the PS shuttle and electrode structural integrity problems. To tackle these problems, polymer-based strategies have recently demonstrated encouraging potential with the success of a polymer binder and separators in Li–S batteries. Multifunctional polymer binders such as gum arabic,[10] gelatin[11] and PEO,[12] among others, have demonstrated great effectiveness in maintaining electrode integrity and in confining PSs within the cathodic chamber, whereas the use of a functionalized polymer separator also revealed significant PS shuttle suppression by blocking the penetration of the PS to the anode.[13,14]

Polybenzimidazole (PBI) (Scheme 1), which has a high melting point, has been extensively used in high-performance protective applications such as firefighter implements, astronaut space suits and aircraft wall fabrics, among others, owing to its superior stability and retention of mechanical strength at elevated temperatures.[15,16] Traditional PBI is synthesized by a condensation reaction of diphenyl isophthalate and 3,3′,4,4′-tetraaminodiphenyl.[17] The spontaneous

[1]College of Chemical and Biological Engineering, Zhejiang University, Hangzhou, China; [2]Department of Chemistry, Hefei National Laboratory for Physical Science at Microscale, University of Science and Technology of China, Hefei, China and [3]Centre for Clean Environment and Energy, Environmental Futures Research Institute and Griffith School of Environment, Griffith University, Nathan, Queensland, Australia
Correspondence: Professor Z Li, College of Chemical and Biological Engineering, Zhejiang University, 38 Zheda Rd, Xihu, Zhejiang, Hangzhou 310027, China.
E-mail: zhoupengli@zju.edu.cn
or Professor S Zhang, Centre for Clean Environment and Energy, Environmental Futures Research Institute and Griffith School of Environment, Griffith University, Parklands Drive, Southport, Gold Coast, Queensland 4222, Australia.
E-mail: s.zhang@griffith.edu.au
Received 29 April 2016; revised 26 June 2016; accepted 20 July 2016

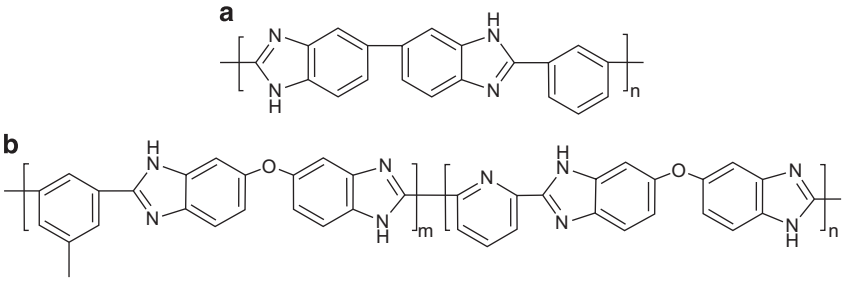

**Scheme 1** Molecular structure of (**a**) traditional polybenzimidazole (PBI) and (**b**) modified PBI (mPBI).

cyclization of the intermediate amino-amide to PBI is beneficial to the highly stable chemical structure. The complexation with phosphoric acid makes PBI an excellent proton conductive membrane material for fuel cells, in combination with its high mechanical, exceptional thermal and electrochemical stability.[18,19] The abundant nitrogen-containing functional groups bestow a great potential for chemical interactions with lithium PSs, similar to those between PBI and phosphoric acid. In addition, functional polymers with pyrrolic and pyridinic N such as polypropylene (PP)[20] and PVP,[21] as well as those with an ether bond such as PEO[22] and polysaccharides[23] could have important roles in capacity retention for Li–S batteries.[24]

Herein, we develop a modified PBI (mPBI) polymer (Scheme 1) as a binder and a separator functional reagent for Li–S batteries. As a binder, the as-prepared mPBI polymer provides resilient adhesion and mechanical strength for the sulfur cathode. The ether bonds and additional pyridine units on the mPBI polymer facilitate chemical interactions with PS, and, therefore, effectively restrain active sulfur within the cathode. The proton conductivity of mPBI manifested in proton exchange membrane fuel cells suggests a great potential of fast $Li^+$ ion transport and improved electrochemical kinetics for the corresponding sulfur electrodes. Furthermore, mPBI is immobilized onto the separator to graft the aforementioned functions to the separator. Owing to the additional ionic selectivity property, mPBI literally builds a blocking layer on the separator to prevent PS from leaching into the anodic region, further suppressing PS shuttling during the charge–discharge process. The proposed dual actions of mPBI on the binder and separator may address the problems of sulfur dissolution, volume expansion and the PS shuttling effect to improve the performance and stability of Li–S batteries.

## MATERIALS AND METHODS

### Material preparation

*Synthesis of mPBI.* 3,3,4,4-tetraaminodiphenyl ether (TADPE) monomer was synthesized through a typical four step procedure starting with 4,4-diaminodiphenyl ether.[25] The mPBI was synthesized through a polymerization process of TADPE and 2,6-pyridinedicarboxylic acid (2,6-PDA). Typically 4.7 g TADPE, 3.2 g 2,6-PDA and 0.2 g trimesic acid were added into the flask containing polyphosphoric acid and $P_2O_5$. The mixture was stirred at ambient temperature for 30 min and subsequently heated to 200 °C for another 10 h under a $N_2$ atmosphere. The obtained brunet viscous product was poured into deionized water, and the precipitate was filtered, washed with deionized water and dilute alkali solution until the filtrate PH = 7, and vacuum dried at 80 °C for 12 h.

*Preparation of polymer films.* To investigate the mechanical properties of the polymer binder, polymer films were prepared through a solvent casting method. Typically mPBI or polyvinylidene difluoride (PVDF) was first dissolved in N-methyl-2-pyrrolidone (NMP) with a concentration of 50 mg $ml^{-1}$ under vigorous stirring at 80 °C. The solution was then transferred to a Teflon flat disk and dried at 60 °C for 24 h before the polymer film was peeled off.

*Preparation of $Li_2S_4$@binder films.* $Li_2S_4$@binder films were fabricated to investigate the PS dissolution behavior with different polymer binders. The $Li_2S_4$@binder solution was obtained by adding sulfur and $Li_2S$ in a proportion of 3:1 into the as-prepared binder/NMP solution. The weight ratio of $Li_2S_4$ to binder was 1:1. The $Li_2S_4$ and binder contents were kept the same for PVDF- and mPBI-based samples for comparison. The obtained solution was slowly evaporated at 60 °C until a homogeneous film was obtained. To prepare $Li_2S_4$@binder electrodes for cell cycling, super P was added as a conductive matrix into the prepared $Li_2S_4$@binder solutions ($Li_2S_4$: mPBI: super P = 1:1:1 in weight). The solutions were stirred and dried at 60 °C until self-standing electrodes were obtained. All of the procedures were performed in an Ar-filled glove box.

*Preparation of the mPBI–PP separator.* The mPBI-functionalized (mPBI–PP) separator was prepared by coating mPBI/NMP solution on the surface of Celgard (Charlotte, NC, USA) membranes with different mPBI loadings of 0.3, 0.5, 1.0 and 3.0 mg $cm^{-2}$ and slowly drying the membranes for 12 h at 60 °C.

### Characterization

*Mechanical measurement.* The prepared polymer films were cut into dumbbell shapes for tensile measurement. The stress–strain data of the mPBI and PVDF films were collected by a Roell Z020 universal materials tester (Zwick, Ulm, Germany) with a preloading force of 0.5 N and a trial speed of 5 mm $min^{-1}$ under ambient temperature. Trouser-shaped polymer films were prepared for the tearing test.[26] A cut was made at the center of the width of the specimen. The trouser legs were inserted symmetrically and in axial alignment with the direction of the pull in each grip. Specimens were tested at a strain rate of 20 mm $min^{-1}$. For the adhesive test, two aluminum plates were lap splice bonded by a polymer binder with a bond area of $2 \times 2$ cm and pulled in opposite directions until they were exfoliated with a preloading force of 5 N and strain rate of 1 mm $min^{-1}$.

*Spectroscopic measurements.* For the spectroscopic tests, $Li_2S_4$ solution was first prepared by mixing proportionally elemental sulfur and $Li_2S$ in NMP under vigorous stirring for 12 h. $Li_2S_4$ sample was collected after evaporating the solvent. The PS-treated sample ($Li_2S_4$-mPBI) was obtained by adding a proportional amount of S and $Li_2S$ into mPBI/NMP solution and dried under the same condition as $Li_2S_4$. The $Li_2S_4$-mPBI was washed with tetrahydrofuran (THF) to remove unbounded $Li_2S_4$ before testing. X-ray photoelectron spectroscopy was acquired in an ESCALAB 250Xi X-ray photoelectron spectrometer (ThermoFisher, Renfrew, UK) operating with an Al Kα radiation source, with an energy resolution of 1 eV for the survey and 0.6 eV for individual characteristic peaks. The ultraviolet–visible absorption data of the $Li_2S_4$ binder in NMP were collected by a Cintra 303 (GBC, Melbourne, VIC, Australia) spectrophotometer with a scan rate of 200 nm $min^{-1}$ and resolution of 0.08 nm. A quartz vessel was used for ultraviolet–vis measurement. Blank NMP was used as a reference. Fourier transform infrared spectrometry analysis was performed using a Tensor 27 (Bruker, Karlsruhe, Germany). The sample was mixed with KBr in a weight ratio of 1:100 and pressed into a pellet under a pressure of 10 MPa. Each spectrum was collected at a resolution of 4 $cm^{-1}$ from 4000 to 400 $cm^{-1}$.

*Scanning electron microscope (SEM).* The morphologies of the sulfur electrodes and separators were observed by an Utral 55 field-emission SEM microscope

(CorlzeisD, Oberkochen, Germany). The in-lens secondary electron detector was used with an accelerating voltage of 5 kV and a working distance of ~7 mm.

### Electrochemical evaluation

The hierarchical macroporous carbon was synthesized as previously reported.[27] Sulfur macroporous composite was prepared via thermal treatment of the ball-milled mixture of sulfur and macroporous carbon with a mass ratio of 7:3 at 155 °C for 4 h in an $N_2$ atmosphere. The working electrode was fabricated by casting the slurry containing sulfur macroporous composite, super P and polymer binder in a weight ratio of 7:2:1 on an aluminum foil and vacuum drying at 60 °C for 12 h. The sulfur loading on the electrode was controlled at ~1 mg cm$^{-2}$. Increased sulfur loadings of 2.0, 4.5, 5.8 and 7.2 mg cm$^{-2}$ for mPBI-based electrodes were also prepared for higher areal capacities. Coin cells (CR2025) were assembled in an Ar-filled glove box using lithium foil as the counter electrode and a PP membrane (or mPBI–PP membrane) as the separator. The electrolyte consisted of lithium bis (trifluoromethane sulfonimide) (LiTFSI, 1 mol l$^{-1}$) and $LiNO_3$ (1 wt%) in DOL-DME binary solvent (1:1 ratio in volume, DOL: 1,3-dioxolane, DME: 1,2-dimethoxyethane). A total of 50 µl mg$^{-1}$ s of electrolyte was added to each cell. The electrochemical performance of the sulfur electrodes were tested by galvanostatic charge/discharge using LAND battery testers (Wuhan, China). Current density and specific capacity were calculated based on the mass of S active material. Cyclic voltammetry (CV) data were collected with a CHI604E electrochemical workstation (CH Instruments, Shanghai, China) in the voltage range of 1.8–2.6 V vs $Li^+$/Li at a scan rate of 0.1 mV s$^{-1}$. Electrochemical impedance spectroscopy was recorded by a CHI604E electrochemical workstation (CH Instruments) with an amplitude of 5 mV in the frequency range of 0.01–100 kHz.

## RESULTS AND DISCUSSION

### mPBI as binder

The as-synthesized mPBI consists of imidazole, diphenyl ether and pyridine structural units as shown in Scheme 1. PVDF and mPBI films with the same thickness were prepared for tensile measurement to investigate the mechanical properties of mPBI compared with those of the traditional PVDF binder. mPBI can be readily prepared into a film with a light brown-yellow color. Figure 1a shows the visual appearances of the mPBI and PVDF films. The tensile test revealed that the mPBI film has three times higher yield strength, five times higher modulus of elasticity and four times higher fracture strength than PVDF, as shown in Figure 1b and Supplementary Table S1. The tearing and adhesive tests also demonstrated that mPBI is able to deliver a consistently higher tearing tolerance and much higher adhesive strength than PVDF (Supplementary Figure S1). The preferable stress–strain behavior of mPBI is attributed to the cross-linked molecular structure, which provides high physical strength, whereas

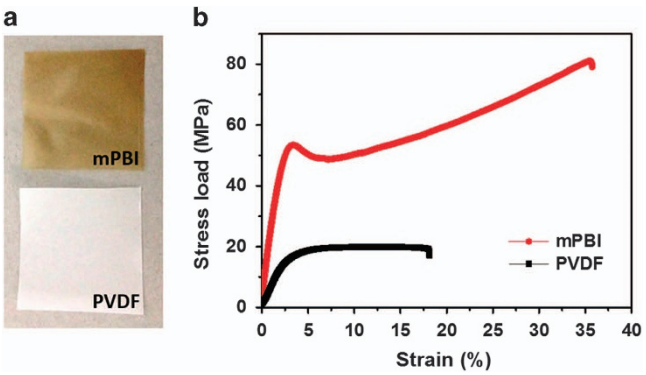


**Figure 1** (**a**) Photograph and (**b**) stress–strain curves of the as-prepared modified polybenzimidazole (mPBI) and PVDF films.

the ether bond provides favorable suppleness. Overall, the mechanical measurements reveal the superb mechanical properties of the mPBI sample, which endow it with the ability to maintain the strong structural integrity of the corresponding sulfur electrodes, suggesting that mPBI is a promising material as a binder for Li–S batteries.

To investigate the chemical interaction between mPBI and sulfur species, a series of spectroscopic measurements of pure $Li_2S_4$, mPBI and PS-treated mPBI (that is, $Li_2S_4$-mPBI) samples were performed, and the corresponding spectra are shown in Figure 2. Compared with the pristine mPBI spectrum, the $Li_2S_4$-treated sample demonstrates a distinctly weakened peak at 3421 cm$^{-1}$ and a peak set ~2922 cm$^{-1}$ in the fourier transform infrared spectrometry spectra (Figure 2a), which are assigned to the stretching vibration of isolated N-H and the self-associated N-H, respectively.[28] The C=N stretching vibration peak undergoes a blue shift from 1625.8 to 1654.8 cm$^{-1}$, whereas the other two vibrations, which are at 1384 and 1049 cm$^{-1}$, corresponding to aryl C-N stretching and alkyl C-N stretching, respectively,[29] almost disappear compared with the spectrum of the untreated mPBI. The changes to the nitrogen relevant peaks are attributed to the formation of the coordinated N-Li-S bond.[30,31] It should be noted that several new peaks at 1304, 667 and 500 cm$^{-1}$ are ascribed to the S=O, C-S and S-S stretching vibrations, respectively.[10,32] This finding clearly suggests that mPBI is able to chemically adsorb PS via these chemical bonds. The chemical bonds between PS and mPBI can also be verified in the ultraviolet–vis spectroscopic investigation. In the ultraviolet–vis spectrum in Figure 2b, the $Li_2S_4$-mPBI sample exhibits a new absorption peak at 550 nm compared with the pure $Li_2S_4$ and mPBI samples. The X-ray photoelectron spectroscopy measurement further provides evidence of the mPBI–PS interaction. The bare $Li_2S_4$ typically contributes an overlapped peak pair in the S 2p spectrum at 160.5 and 163.5 eV, which refers to terminal sulfur and bridging sulfur atoms, respectively.[33] Compared with the bare $Li_2S_4$ sample, both the terminal sulfur and the bridging sulfur in the $Li_2S_4$-mPBI sample shift to a higher binding energy by 1.0 and 0.5 eV, respectively (Figure 2c), indicating a decrease of the electron density on the sulfur atoms. This decrease is ascribed to the interaction between sulfur and nitrogen in mPBI in the form of N-Li-S.[34] More significantly, a new overlapped peak pair emerges in the range of 166–171 eV, which refers to the thiosulfate and polythionate species,[35] demonstrating the chemical bond between mPBI and $Li_2S_4$. The excellent agreement with the chemical interactions between mPBI and PS suggests its potential effectiveness in constraining sulfur-containing species within the cathode and inhibiting PS from dissolving and migrating to the anode chamber.

Freestanding composite films were prepared by slow evaporation of a homogeneous NMP mixture slurry containing an equal amount of the binder and $Li_2S_4$, namely $Li_2S_4$@PVDF and $Li_2S_4$@mPBI composite films. For the purpose of direct verification of the PS adsorption capability of the binders, the $Li_2S_4$ dissolution behaviors of these two films are compared in Figure 3a. The obtained films were immersed into same amount of electrolyte and observed after different times. The electrolyte with the $Li_2S_4$@mPBI film was limpid and clear after 24 h, whereas the solution with $Li_2S_4$@PVDF showed a yellow color immediately after the immersion and turned to a dark red-brown after 24 h of dissolution. This phenomenon also suggests that more $Li_2S_4$ is leached from $Li_2S_4$@PVDF than that from $Li_2S_4$@mPBI and intuitively indicates that mPBI has a much higher PS retention than does the PVDF binder. The electrochemical stability of mPBI was verified by a cyclic voltammetry test before the electrochemical characterizations for the mPBI-based electrodes. No obvious redox peaks for the pure mPBI electrode in the potential range of 1.5–3.0 V (vs $Li^+$/Li, hereafter

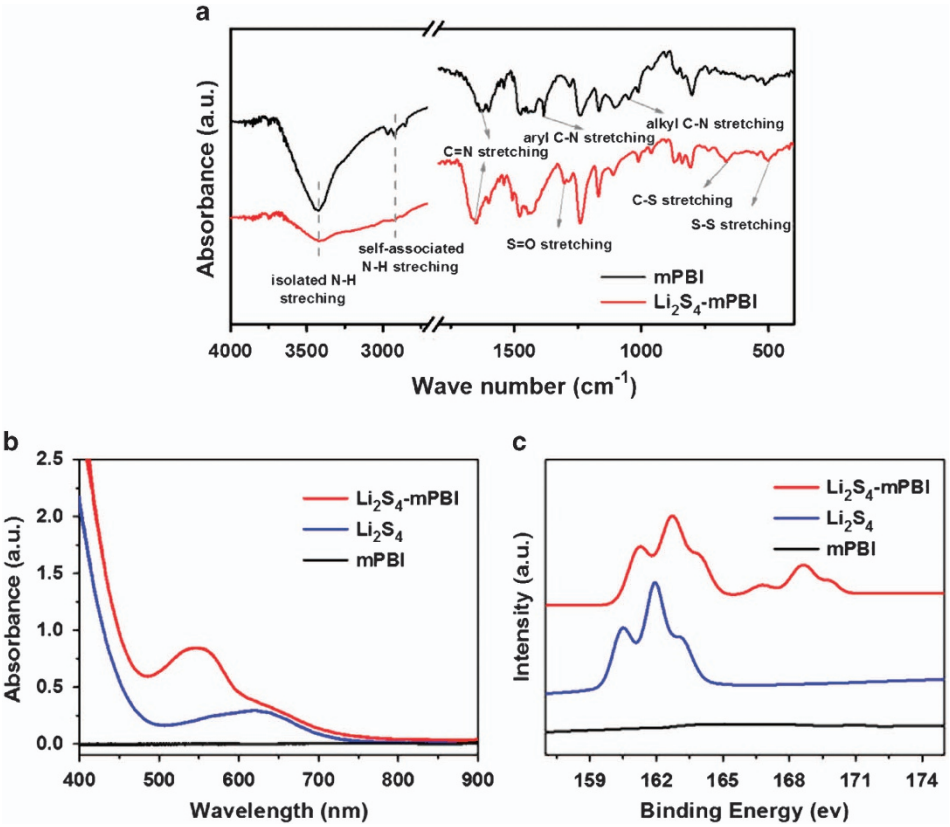


**Figure 2** Chemical interaction between polysulfide and modified polybenzimidazole (mPBI). (**a**) Fourier transform infrared spectrometry spectra of the as-prepared mPBI and $Li_2S_4$-mPBI samples, (**b**) ultra violet–visible spectra and (**c**) S 2p core spectra of the mPBI, $Li_2S_4$ and $Li_2S_4$-mPBI samples.

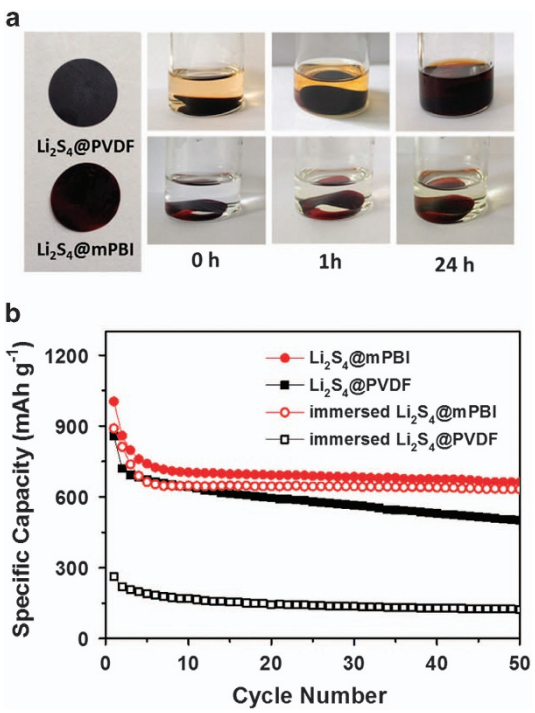


**Figure 3** (**a**) Visual observation of the as-prepared $Li_2S_4$@binder composite films and their dissolution behaviors in electrolyte solution. (**b**) Cycling performance comparison at C/5 (0.235 mA $cm^{-2}$) of the as-prepared $Li_2S_4$@binder electrodes before and after immersion in the electrolyte. The sulfur loading on the electrodes is ca. 0.7 mg $cm^{-2}$.

inclusive) were observed, as shown in Supplementary Figure S2, revealing the excellent electrochemical inertness of the obtained mPBI. Figure 3b shows that the cell fabricated with the as-prepared $Li_2S_4$@mPBI films clearly delivers larger capacity and better stability than those with the as-prepared $Li_2S_4$@PVDF films, which is in line with the observation of the $Li_2S_4$ dissolution behavior comparison experiment shown in Figure 3a. Furthermore, after both as-prepared $Li_2S_4$ electrodes were immersed in the electrolyte, the immersed $Li_2S_4$@mPBI film presented a much higher capacity than the immersed PVDF@$Li_2S_4$ film, which again verifies that the mPBI binder is superior for PS adsorption and re-utilization.

Sulfur electrodes were prepared by mixing the sulfur–carbon composite[27] with the mPBI or PVDF binder and denoted as S@mPBI and S@PVDF electrode, respectively. To evaluate the effectiveness of the physical and chemical functions of mPBI as the binder in Li–S batteries, galvanostatic charge–discharge tests were conducted. A summary of the cell testing conditions and the corresponding areal capacities for the as-prepared sulfur electrodes is provided as shown in Supplementary Table S2. The charge–discharge profile of the S@mPBI electrode shows two typical discharge platforms within the range of 1.8–2.6 V, as shown in Figure 4a, which are ascribed to the two stages of sulfur reduction; that is, the formation of soluble long-chain PSs ($Li_2S_x$, $4 \leqslant x \leqslant 8$) at ca. 2.3 V and an insoluble short-chain $Li_2S_2$/$Li_2S$ at ~2.1 V. The redox peaks of the cyclic voltammetry curve in Figure 4b fittingly conform to the plateaus in the charge/discharge profile. When scanning forward, the peaks near 2.4 V are attributed to the electro-oxidations of $Li_2S_2$/$Li_2S$ to higher-ordered PSs, whereas the two peaks at 2.35 and 2.05 V when scanning backwards represent the reduction of sulfur to soluble higher-ordered PSs ($Li_2Sx$, $4 \leqslant x \leqslant 8$), which are

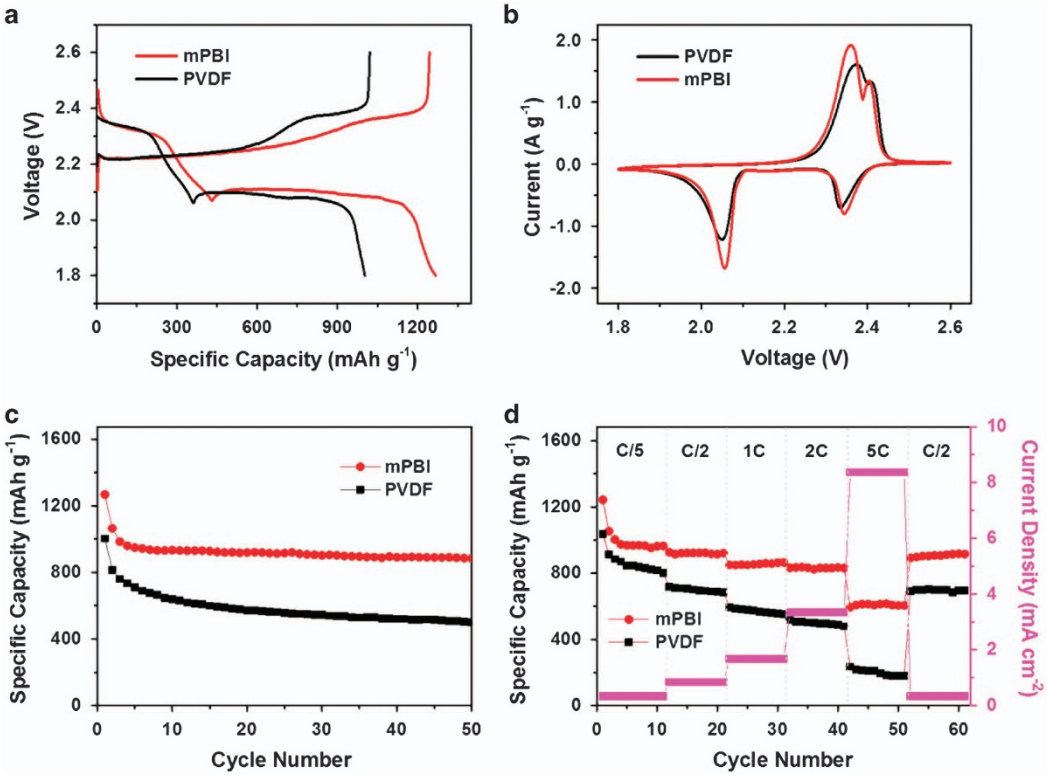


**Figure 4** Electrochemical performance of the S@PVDF and S@mPBI electrode. (**a**) Typical charge–discharge profiles, (**b**) the cyclic voltammetry curves at a scan rate of 0.1 mV $s^{-1}$ of the S@mPBI electrode, (**c**) the cycling performance at C/5 (0.34 mA $cm^{-2}$) and (**d**) multi-rate performance of the PVDF- and mPBI-based electrodes. The sulfur loading on the electrodes is ca. 1.0 mg $cm^{-2}$. mPBI, modified polybenzimidazole.

further reduced into $Li_2S_2$ and $Li_2S$, respectively. Compared with the conventional S@PVDF electrode, the S@mPBI electrode exhibits a higher capacity and improved electrode kinetics owing to the smaller potential gap between the charge and discharge platforms in the voltage profile, as well as that between the redox peaks in cyclic voltammetry curves. The coin cell cycling test (Figure 4c) demonstrates that the S@mPBI electrode delivers significantly better specific capacity and rate capability than does the S@PVDF electrode, suggesting the superiority of the mPBI binder for improving the cycling performance of the sulfur electrode compared with the commercial PVDF binder. In particular, the S@mPBI electrode conveys an initial discharge capacity of 1267 mAh $g^{-1}$ (1.27 mAh $cm^{-2}$) and a highly reversible capacity of 885 mAh $g^{-1}$ (0.89 mAh $cm^{-2}$) after 50 cycles deep charge/discharges at C/5 (0.34 mA $cm^{-2}$) current density (1C = 1675 mA $g^{-1}$ s). This result represents significantly improved electrochemical performance compared with that of the S@PVDF electrode (Figure 4d). The effect of lower electrolyte volumes (that is, 5, 15 and 30 µl $mg^{-1}$ s) on electrode performance at a sulfur loading of ca. 1.0 mg $cm^{-2}$ was investigated as shown in Supplementary Figure S3.The Li–S cell with the addition of 5 µl $mg^{-1}$ s electrolyte exhibited almost no capacity at C/5 owing to the incomplete electrode wetting and the resultant large electrochemical impedance. This situation was improved when the electrolyte addition increased to 15 and 30 µl $mg^{-1}$ s. Nevertheless, compared with that with 50 µl $mg^{-1}$ s, the samples with lower electrolyte amounts still showed relatively higher electrochemical polarization and lower sulfur utilizations, whereas a higher electrolyte addition of 80 µl $mg^{-1}$ s led to slightly faster capacity decay. To investigate the degree of the PS shuttle suppression, electrodes with different binders were cycled using electrolyte without a $LiNO_3$ additive. As expected, the S@mPBI electrode offers superior cycling stability and significantly enhanced coulombic efficiency (93.1% vs 81.5%) after 50 cycles than does the S@PVDF electrode (Supplementary Figure S4). The surface morphology of the sulfur electrodes before and after cycling observed by SEM also reveals that less PS is re-deposited on the carbon surface, as shown in Supplementary Figure S5, suggesting that the PS shuttle is inhibited for the S@mPBI electrode. A multi-rate cycling test was performed to investigate the high rate performance of the sulfur electrodes. The S@mPBI electrode achieves a highly reversible capacity of 610 mAh $g^{-1}$ (0.61 mAh $cm^{-2}$) at a high discharge rate of 5 C (8.38 mA $cm^{-2}$) owing to the preferable ion conductivity of mPBI and recovers to 910 mAh $g^{-1}$ (0.91 mAh $cm^{-2}$) when the test current is switched back to C/5 (0.34 mA $cm^{-2}$). However, for the S@PVDF electrode, the capacity decreases rapidly as the discharge current increases.

The electrochemical impedance spectroscopy measurements are consistent with the results of the multi-rate tests. In particular, the S@mPBI electrode possesses smaller impedance and faster reaction kinetics before and after cycling than does the S@PVDF electrode (Supplementary Figure S6). The superior electrochemical performance of the S@mPBI electrode can be attributed to the fact that the mPBI binder is capable of confining the sulfur and PS within the cathode via its inherent PS chemical adsorption ability and by preserving electrode integrity owing to excellent mechanical strength.

### mPBI functionalized separator

Apart from its excellent performance as a binder for the sulfur electrode, mPBI also possesses great potential for the functionalization of the separator to tackle the shuttle problem for Li–S batteries. The

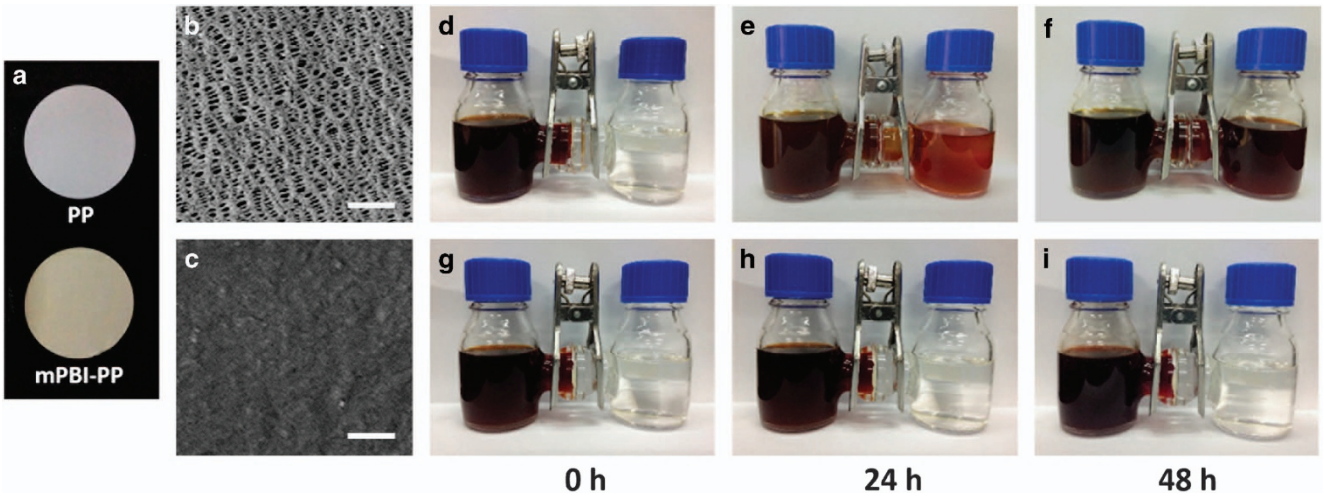


**Figure 5** (**a**) Optical images of the pristine polypropylene (PP) membrane and the modified polybenzimidazole.(mPBI–PP) membrane. SEM comparisons between (**b**) the pristine PP membrane and (**c**) the mPBI–PP membrane. The scale bar equals to 1 μm. Visual comparison of polysulfide diffusion in double-cell reactor with (**d**–**f**) PP separator or (**g**–**i**) mPBI–PP separator at different times.

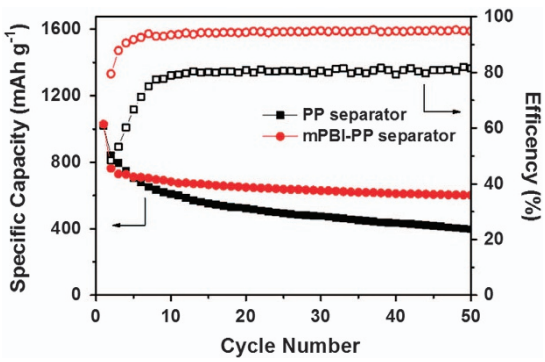


**Figure 6** Comparison of columbic efficiency and cycling performance of sulfur electrodes with sulfur loading of ca. 1.0 mg cm$^{-2}$ at C/5 (0.34 mA cm$^{-2}$) using pristine polypropylene (PP) or the modified polybenzimidazole (mPBI–PP) membrane as a separator in an electrolyte without $LiNO_3$.

commercial Celgard PP membranes with pores of nanometer sizes (Figure 5a–b) are predominately used as separators for Li-ion and Li–S batteries in state-of-the-art manufacturing, research and development.[36] The PP separator has excellent wettability but has zero retention force with respect to PS. Owing to the driving force from the concentration gradient and electro-osmotic effect, PS anions tend to diffuse with $Li^+$ anions from the cathode to the anode through the separator during the charge–discharge process, leading to the so-called 'polysulfide shuttling effect'. Concerning this issue, an anion repulsive membrane could relieve the shuttling effect to some extent, which is similar to proton exchange membrane fuel cells.[37] The performance of the resultant Li–S batteries could be further improved. Herein, we attempt to introduce a second blocking mechanism to eliminate the PS shuttling effect by grafting the functions of the mPBI binder to the conventional non-selective PP separator. The functionalization of the PP membrane with the mPBI polymer offers some advantages: first, the mechanical properties of the resultant membrane will be significantly reinforced as the mPBI polymer has excellent mechanical properties. This reinforcement could help protect the separator from being pierced by the Li dendrite formed during cycling. Second, and more importantly, it is expected that the PS adsorption capability of mPBI is amalgamated with the PP membrane to prevent the PS penetration through the separator. However, the side effects of such a separator modification method must be taken into our consideration: it might reduce electrolyte wettability, increase electrochemical impedance and lessen active material utilization in batteries owing to the reduced pore size and increased thickness of the separator.[38,39] In this work, we aim to establish a PS shield onto the separator without jeopardizing the wettability and ionic conductivity of the membrane.

The mPBI-functionalized PP membrane (mPBI–PP) was prepared by coating mPBI/NMP solution onto the cathodic side of PP separator (Celgard 2400) with an mPBI loading of 0.5 mg cm$^{-2}$. The homogeneous distribution of mPBI on the PP membrane was confirmed by visual observation and SEM (Figure 5c). No contamination occurred as no mPBI was observed on the anodic side (Supplementary Figure S7). The PS blocking effect was investigated by comparing the PS diffusion behavior with the pristine PP separator and mPBI–PP separator in an H-type cell as shown in Figure 5d–i. About 0.5 M $Li_2S_4$ dissolved in electrolyte containing 1 M LiTFSI in a binary solvent of DME and DOL (1:1 in volume ratio) was pre-prepared and filled in one chamber, whereas the pure electrolyte filled the other. The PP or resultant mPBI–PP membrane was used as a separator between the two chambers, as shown in Figures 5d and g, respectively. In the case of the pristine PP separator, the color changed from colorless to a brownish-red within 24 h and to dark brown within 48 h, as shown in Figure 5e and f, respectively, indicating that the PS penetrated the separator and migrated to the opposite chamber. In contrast, with the mPBI–PP separator, the opposite chamber was kept clear and remained almost colorless even after as long as 24 and 48 h, as shown in Figure 5h and i, respectively. The comparison directly demonstrates the excellent PS shielding capability of the mPBI–PP separator. The PS blocking effect of the mPBI–PP separator is attributed to the aforementioned chemical bond between mPBI and PS. Similar to the bonding of traditional PBI with phosphoric acid, an anion (that is, the PS anion) repelling shield could be built on the cathodic surface of the separator. Therefore, the chemical interaction of PS with mPBI forms a negatively charged PS layer on the separator surface that repels PS anions. As a result, the shuttle of PSs is prohibited, even after the adsorption sites of mPBI are saturated.

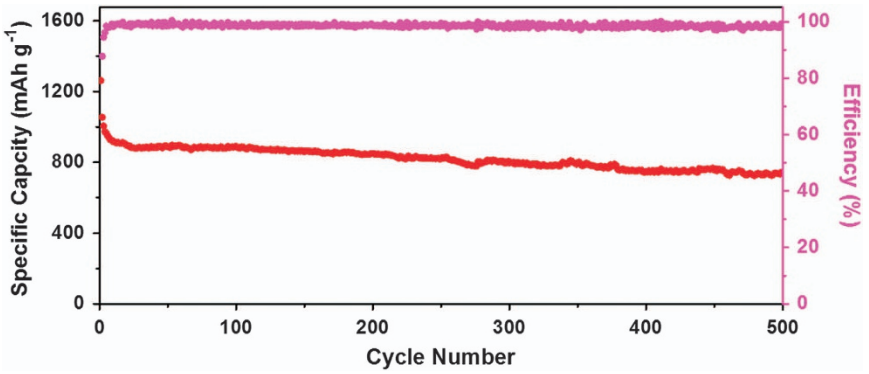


**Figure 7** Long-term cycling performance of the Li–S cell with the mPBI binder and the mPBI–PP separator at C/5 (0.34 mA $cm^{-2}$) at room temperature. The sulfur loading on the electrode is ca. 1.0 mg $cm^{-2}$. mPBI, modified polybenzimidazole; PP, polypropylene.

To verify the shuttle inhibition of the mPBI–PP separator, a sulfur electrode based on the PVDF binder was cycled using the separator with or without mPBI in electrolyte without $LiNO_3$ additive, as shown in Figure 6. The open circuit voltages of the Li–S cells with the mPBI–PP separator are in the range of 2.7–3.1 V. A much higher columbic efficiency (~95%) and capacity retention were achieved for electrodes with the mPBI–PP separator than with the pristine PP separator. This result indicates that the mPBI–PP separator possesses a great capability for suppressing PS shuttling and improving the cyclability of the sulfur cathode. The mPBI loading on the mPBI–PP separator has a critical role in the cycling performance and coulombic efficiency of the sulfur cathode (Supplementary Figure S8). An insufficient loading of mPBI leads to insignificant PS shielding, whereas excessive loading results in poor $Li^+$ transmission owing to the much lower ion conductivity of mPBI compared with that of the liquid electrolyte.

For practical applications, a broad operating temperature range is a desirable feature. The excellent thermo-mechanical and thermo-chemical stabilities of mPBI provide Li–S batteries with the potential to perform well and safely in a wide range of temperatures. This performance can be demonstrated by the high operation temperature (60 °C) test shown in Supplementary Figure S9. With its mPBI binder and mPBI–PP separator, the resultant Li–S cell demonstrates significantly superior cycling performance at 60 °C. In strong contrast, the Li–S cell with the PVDF binder and the pristine PP separator showed a much faster capacity decay and lower reversible capacity. It is also well recognized that a useful sulfur cathode shall possess high sulfur loading. The conventional PVDF binder is usually unable to achieve a sulfur loading of $>3$ mg $cm^{-2}$[40] owing to its poor adhesion strength, which leads to the cracking and detachment of the active material in electrode fabrication, as well as the electrode structural collapse during the cycling process. With the excellent mechanical properties of the mPBI binder, a high sulfur loading of 7.2 mg $cm^{-2}$ can be achieved with a highly reversible areal capacity of 5.2 mAh $cm^{-2}$ (Supplementary Figure S10a), which surpasses that of currently commercialized Li-ion batteries.[41] The voltage profile comparison reveals an aggravated electrochemical polarization with the increase of sulfur loading according to the declined discharge voltage plateaus (Supplementary Figure S11). In addition, the electrode capacities deteriorated from the first cycle to subsequent cycles when the S loading was low (that is, 2 mg $cm^{-2}$). In strong contrast, the activation process of the electrode was observed to be that the discharge voltage increased with the cycling number when the sulfur loading was high, that is, 7.2 mg $cm^{-2}$. The thicknesses of the electrodes with different sulfur loadings were observed by SEM (Supplementary Figure S12). On the basis of the obtained thicknesses, the volumetric capacities of the electrodes are also obtained, as shown in Supplementary Figure S10b. The S@mPBI electrode with a sulfur loading of 2.0 mg $cm^{-2}$ exhibits the highest volumetric capacity of 330 Ah $l^{-1}$. Furthermore, a thickness comparison between the as-prepared S@mPBI electrode and the state-of-art Ni-Mn-Co (NMC) electrode was performed.[42] The S@mPBI electrode requires a close thickness of 50 μm to achieve a similar areal capacity of ~1.6 mAh $cm^{-2}$ compared with the NMC electrode, revealing the great practical prospect of the obtained Li–S batteries.

The long-term cycling performance of the resultant Li–S cell was also evaluated based on the mPBI binder and the functionalized separator (Figure 7). The excellent mechanical property of mPBI, combined with the double suppression of PS shuttling via the PS adsorption offered by the mPBI binder and the mPBI–PP separator grants the Li–S battery with the remarkable cycling performance and excellent capacity retention of 750 mAh $g^{-1}$ (0.75 mAh $cm^{-2}$), even after 500 deep charge–discharge cycles with cyclic decay of $<0.08\%$ per cycle and high coulombic efficiency above 98%. It should be noted that both a high coulombic efficiency of ~95% and a decent capacity of $>600$ mAh $g^{-1}$ were achieved using the mPBI–PP separator in electrolyte with no $LiNO_3$ owing to its excellent PS blocking effect, as demonstrated in Figure 6. It has been well established that $LiNO_3$ can help develop a stable protective solid electrolyte interlayer (SEI) on a lithium anode surface,[43] which is capable of protecting the anode against the trace amount of PSs that escaped through the separator; thus, $LiNO_3$ is still used in this work. The achievement of high coulombic efficiency and the significant extension of cell lifespan suggests that $LiNO_3$ continues to have a vital role in the long-term operation of the ether-based Li–S system.

## CONCLUSION

mPBI was developed for the first time as a binder and as an agent to functionalize the separator for Li–S batteries. The excellent mechanical features and abundant chemical interactions with PS of the mPBI binder have critical roles in maintaining electrode integrity and restraining PS from dissolving into the electrolyte. The mPBI-functionalized separator is highly effective in suppressing the PS anion from shuttling to the Li anode. Because of the dual actions of the mPBI polymer, the as-prepared Li–S battery delivered remarkably improved performance and cycling stability; that is, a high reversible capacity of 750 mAh $g^{-1}$ (0.75 mAh $cm^{-2}$) after 500 cycles at C/5 (0.34 mA $cm^{-2}$) with a cyclic decay of 0.08% per cycle. The

findings of this work suggest that the functionalization of the binder and the separator is a practical and low-cost strategy to tackle the long-standing problem of Li–S batteries. This work also offers a promising strategy for other advanced energy storage devices, for example, Li-ion batteries, Li-air batteries and supercapacitors.

## CONFLICT OF INTEREST

The authors declare no conflict of interest.

## ACKNOWLEDGEMENTS

This work is financially supported by the National Natural Science Foundation of China, Grant Nos. 21476200 and 21276229; funds from the Science & Technology Ministry of Zhejiang province, 2014C31003; and a research grant from the Australia Research Council Discovery Projects.

1 Dunn, B., Kamath, H. & Tarascon, J. M. Electrical energy storage for the grid: a battery of choices. *Science* **334**, 928–935 (2011).
2 Goodenough, J. B. & Kim, Y. Challenges for rechargeable Li batteries. *Chem. Mater.* **22**, 587–603 (2010).
3 Lian, P. C., Zhu, X. F., Liang, S. Z., Li, Z., Yang, W. S. & Wang, H. H. High reversible capacity of $SnO_2$/graphene nanocomposite as an anode material for lithium-ion batteries. *Electrochim. Acta* **56**, 4532–4539 (2011).
4 Chu, S. & Majumdar, A. Opportunities and challenges for a sustainable energy future. *Nature* **488**, 294–303 (2012).
5 Zhan, L., Wang, S. Q., Ding, L. X., Li, Z. & Wang, H. H. Grass-like $Co_3O_4$ nanowire arrays anode with high rate capability and excellent cycling stability for lithium-ion batteries. *Electrochim. Acta* **135**, 35–41 (2014).
6 Bruce, P. G., Freunberger, S. A., Hardwick, L. J. & Tarascon, J. M. Li-$O_2$ and Li-S batteries with high energy storage. *Nat. Mater.* **11**, 19–29 (2012).
7 Yin, Y. X., Xin, S., Guo, Y. G. & Wan, L. J. Lithium-sulfur batteries: electrochemistry, materials, and prospects. *Angew. Chem. Int. Ed.* **52**, 13186–13200 (2013).
8 Yang, Y., Zheng, G. Y. & Cui, Y. Nanostructured sulfur cathodes. *Chem. Soc. Rev.* **42**, 3018–3032 (2013).
9 Evers, S. & Nazar, L. F. New approaches for high energy density lithium-sulfur battery cathodes. *Acc. Chem. Res.* **46**, 1135–1143 (2013).
10 Li, G. R., Ling, M., Ye, Y. F., Li, Z. P., Guo, J. H., Yao, Y. F., Zhu, J. F., Lin, Z. & Zhang, S. Q. Acacia senegal-inspired bifunctional binder for longevity of lithium-sulfur batteries. *Adv. Energy Mater.* **5**, 1500878 (2015).
11 Sun, J., Huang, Y. Q., Wang, W. K., Yu, Z. B., Wang, A. B. & Yuan, K. G. Application of gelatin as a binder for the sulfur cathode in lithium-sulfur batteries. *Electrochim. Acta* **53**, 7084–7088 (2008).
12 Lacey, M. J., Jeschull, F., Edstrom, K. & Brandell, D. Why PEO as a binder or polymer coating increases capacity in the Li-S system. *Chem. Commun.* **49**, 8531–8533 (2013).
13 Cai, W. L., Li, G. R., He, F., Jin, L. M., Liu, B. H. & Li, Z. P. A novel laminated separator with multi functions for high-rate dischargeable lithium-sulfur batteries. *J. Power Sources* **283**, 524–529 (2015).
14 Huang, J. Q., Zhang, Q., Peng, H. J., Liu, X. Y., Qian, W. Z. & Wei, F. Ionic shield for polysulfides towards highly-stable lithium-sulfur batteries. *Energy Environ. Sci.* **7**, 347–353 (2014).
15 Vogel, H. & Marvel, C. S. Polybenzimidazoles, new thermally stable polymers. *J. Polym. Sci.* **50**, 511–539 (1961).
16 van Krevelen, D. W. New developments in the field of flame-resistant fibres. *Angew. Makromol. Chem.* **22**, 133–157 (1972).
17 Chung, T. S. A critical review of polybenzimidazoles: historical development and future R&D. *J. Macromol. Sci. Rev. Macromol. Chem. Phys.* **C37**, 277–301 (1997).
18 Rosseinsky, D. R. Encyclopedia of polymer science and engineering. *Nature* **339**, 268–269 (1989).
19 He, R. H., Che, Q. T. & Sun, B. Y. The acid doping behavior of polybenzimidazole membranes in phosphoric acid for proton exchange membrane fuel cells. *Fiber Polym.* **9**, 679–684 (2008).
20 Liang, X., Zhang, M. G., Kaiser, M. R., Gao, X. W., Konstantinov, K., Tandiono, R., Wang, Z. X., Liu, H. K., Dou, S. X. & Wang, J. Z. Split-half-tubular polypyrrole@sulfur@polypyrrole composite with a novel three-layer-3D structure as cathode for lithium/sulfur batteries. *Nano Energy* **11**, 587–599 (2015).
21 Seh, Z. W., Zhang, Q. F., Li, W. Y., Zheng, G. Y., Yao, H. B. & Cui, Y. Stable cycling of lithium sulfide cathodes through strong affinity with a bifunctional binder. *Chem. Sci.* **4**, 3673–3677 (2013).
22 Zhang, S. S. A concept for making poly(ethylene oxide) based composite gel polymer electrolyte lithium/sulfur battery. *J. Electrochem. Soc.* **160**, A1421–A1424 (2013).
23 Wang, J. L., Yao, Z. D., Monroe, C. W., Yang, J. & Nuli, Y. Carbonyl-beta-cyclodextrin as a novel binder for sulfur composite cathodes in rechargeable lithium batteries. *Adv. Funct. Mater.* **23**, 1194–1201 (2013).
24 Frischmann, P. D., Gerber, L. C.H., Doris, S. E., Tsai, E. Y., Fan, F. Y., Qu, X. H., Jain, A., Persson, K. A., Chiang, Y. M. & Helms, B. A. Supramolecular perylene bisimide-polysulfide gel networks as nanostructured redox mediators in dissolved polysulfide lithium-sulfur batteries. *Chem. Mater.* **27**, 6765–6770 (2015).
25 Katritzky, A. R., Yang, Z. J. & Cundy, D. J. An improved large-scale preparation of 3,3′,4,4′-tetraaminodiphenyl ether. *Org. Prep. Proced. Int.* **25**, 478–480 (1993).
26 Hatamleh, M. M. & Watts, D. C. Mechanical properties and bonding of maxillofacial silicone elastomers. *Dent. Mater.* **26**, 185–191 (2010).
27 Li, G. R., Cai, W. L., Liu, B. H. & Li, Z. P. A multi functional binder with lithium ion conductive polymer and polysulfide absorbents to improve cycleability of lithium-sulfur batteries. *J. Power Sources* **294**, 187–192 (2015).
28 Kang, Y., Zou, J., Sun, Z. N., Wang, F. H., Zhu, H., Han, K. F., Yang, W. S., Song, H. H. & Meng, Q. H. Polybenzimidazole containing ether units as electrolyte for high temperature proton exchange membrane fuel cells. *Int. J. Hydrogen Energy* **38**, 6494–6502 (2013).
29 Che, M. L., Chuang, S. & Leu, J. The mechanical property, microstructure, and pore geometry of a methyltrimethoxysilane modified silica zeolite (MSZ) film. *J. Electrochem. Soc.* **159**, G23–G28 (2012).
30 Zhou, G., Paek, E., Hwang, G. S. & Manthiram, A. Long-life Li/polysulphide batteries with high sulphur loading enabled by lightweight three-dimensional nitrogen/sulphur-codoped graphene sponge. *Nat. Commun.* **6**, 7760 (2015).
31 Qiu, Y., Li, W., Zhao, W., Li, G., Hou, Y., Liu, M., Zhou, L., Ye, F., Li, H., Wei, Z., Yang, S., Duan, W., Ye, Y., Guo, J. & Zhang, Y. High-rate, ultralong cycle-life lithium/sulfur batteries enabled by nitrogen-doped graphene. *Nano Lett.* **14**, 4821–4827 (2014).
32 Yuen, C., Ku, S., Choi, P., Kan, C. & Tsang, S. Determining functional groups of commercially available ink-jet printing reactive dyes using infrared spectroscopy. *Res. J. Text Appar.* **9**, 26–38 (2005).
33 Pang, Q., Tang, J. T., Huang, H., Liang, X., Hart, C., Tam, K. C. & Nazar, L. F. A nitrogen and sulfur dual-doped carbon derived from polyrhodanine@cellulose for advanced lithium-sulfur batteries. *Adv. Mater.* **27**, 6021–6028 (2015).
34 Wang, X. F., Gao, Y. R., Wang, J. Z., Wang, Z. X. & Chen, L. Q. Chemical adsorption: another way to anchor polysulfides. *Nano Energy* **12**, 810–815 (2015).
35 Liang, X., Hart, C., Pang, Q., Garsuch, A., Weiss, T. & Nazar, L. F. A highly efficient polysulfide mediator for lithium-sulfur batteries. *Nat. Commun.* **6**, 5682 (2015).
36 Huang, X. S. Separator technologies for lithium-ion batteries. *J. Solid State Electrochem.* **15**, 649–662 (2011).
37 Kreuer, K. D., Paddison, S. J., Spohr, E. & Schuster, M. Transport in proton conductors for fuel-cell applications: simulations, elementary reactions, and phenomenology. *Chem. Rev.* **104**, 4637–4678 (2004).
38 Lee, H., Yanilmaz, M., Toprakci, O., Fu, K. & Zhang, X. A review of recent developments in membrane separators for rechargeable lithium-ion batteries. *Energy Environ. Sci.* **7**, 3857–3886 (2014).
39 Zhang, S. S. A review on the separators of liquid electrolyte Li-ion batteries. *J. Power Sources* **164**, 351–364 (2007).
40 Miao, L. X., Wang, W. K., Yuan, K. G., Yang, Y. S. & Wang, A. B. A lithium-sulfur cathode with high sulfur loading and high capacity per area: a binder-free carbon fiber cloth-sulfur material. *Chem. Commun.* **50**, 13231–13234 (2014).
41 Whittingham, M. S. Lithium batteries and cathode materials. *Chem. Rev.* **104**, 4271–4301 (2004).
42 Mohanty, D., Hockaday, E., Li, J., Hensley, D. K., Daniel, C. & Wood, D. L. Effect of electrode manufacturing defects on electrochemical performance of lithium-ion batteries: cognizance of the battery failure sources. *J. Power Sources* **312**, 70–79 (2016).
43 Zhang, S. S. Role of $LiNO_3$ in rechargeable lithium/sulfur battery. *Electrochim. Acta* **70**, 344–348 (2012).

**This work is licensed under a Creative Commons Attribution 4.0 International License. The images or other third party material in this article are included in the article's Creative Commons license, unless indicated otherwise in the credit line; if the material is not included under the Creative Commons license, users will need to obtain permission from the license holder to reproduce the material. To view a copy of this license, visit http://creativecommons.org/licenses/by/4.0/**

© The Author(s) 2016

Supplementary Information accompanies the paper on the NPG Asia Materials website (http://www.nature.com/am)